Magic density in a self-rephasing ensemble of trapped ultracold atoms

A. Bonnin,[*] C. Solaro,[†] X. Alauze, and F. Pereira dos Santos[‡]
LNE-SYRTE, Observatoire de Paris, Université PSL, CNRS, Sorbonne Université, 61 Avenue de l'Observatoire, 75014 Paris, France

(Received 19 July 2018; revised manuscript received 22 January 2019; published 27 February 2019)

We investigate the collective spin dynamics of a self-rephasing bosonic ensemble of ^{87}Rb trapped in a one-dimensional vertical optical lattice. We show that the combination of the frequency shifts induced by atomic interactions and inhomogeneous dephasing, together with the spin self-rephasing mechanism, leads to the existence of a "magic density": i.e., a singular operating point where the clock transition is first-order insensitive to density fluctuations. This feature is very appealing for improving the stability of quantum sensors based on trapped pseudo-spin-1/2 ensembles. Ramsey spectroscopy of the $|5s\,^2S_{1/2}, F = 1, m_F = 0\rangle \rightarrow |5s\,^2S_{1/2}, F = 2, m_F = 0\rangle$ hyperfine transition is in qualitative agreement with a numerical model based on coupled Bloch equations of motion for energy-dependent spin vectors.

DOI: 10.1103/PhysRevA.99.023627

I. INTRODUCTION

The coherent manipulation of ultracold atoms trapped in optical lattices is of great interest for quantum information processing [1,2], quantum simulation [3], and high-precision measurements. In particular, optical lattices constitute a perfectly relevant framework for the development of highly sensitive and accurate sensors, such as optical lattice clocks [4–7] or inertial sensors [8–10]; sensors which subsequently find many applications for exploring many-body physics [11–13] and various aspects of fundamental physics, such as testing general relativity [14,15], searching for dark matter and drift of fundamental constants [16,17], or probing short-range forces [18–20].

For many of these applications, high accuracy, sensitivity, and stability are required. Accuracy and stability are ensured by isolating, as much as possible, the probed atoms from the external environment and by carefully controlling their interactions with the trapping potentials: by using, e.g., magic wavelengths [21,22] and magic fields [23–25] for which a clock transition is respectively insensitive to ac-Stark shift and Zeeman shift fluctuations. Sensitivity is greatly improved by simultaneously interrogating a large number of atoms, which, in contrast with single-ion experiments, allows for better signal-to-noise ratio when the measurement is limited by quantum projection noise [26]. Unfortunately, with a large number of particles, the atom-atom interactions and the resulting density shift [27,28] may also limit the performance of the atomic sensor by adding deleterious bias, noises, and drifts. Notably, measurements relying on ultracold Fermi atoms, thus being *a priori* immune to such shifts, were shown to be also impacted by *s*-wave (and *p*-wave) collisions when atoms experience an inhomogeneous interrogation field [29–31]. Different cancellation techniques have then been developed, such as tuning the pulse duration in Ramsey [32,33] and Rabi [34] spectroscopy or employing the interaction blockade mechanism [35] in a strongly interacting system. As suggested by this latter mechanism, strong interactions can also be beneficial and instigate interesting phenomena, such as spin squeezing from many-particle entanglement [36], collisional narrowing [37], and, of relevance in the work presented here, spin self-rephasing [38–41].

We explore here the so-called Knudsen regime, where the cumulative effect of the identical spin rotation effect (ISRE) [42], which originates from interactions of indistinguishable particles in a nondegenerate gas, counteracts dephasing by keeping atoms synchronized and preserves the coherence of an atomic ensemble for very long times [38,40]. This collective spin self-rephasing (SSR) mechanism leads to an improved short-term stability of the sensor. In that regime, a thorough understanding and modeling of the collective spin dynamics becomes a major issue in order to also ensure high accuracy and long-term stability.

In this paper, we investigate the collective spin dynamics of a self-rephasing bosonic ensemble of ^{87}Rb trapped in a shallow one-dimensional (1D) vertical optical lattice. We probe the $|5s\,^2S_{1/2}, F = 1, m_F = 0\rangle \rightarrow |5s\,^2S_{1/2}, F = 2, m_F = 0\rangle$ hyperfine transition by standard Ramsey spectroscopy. With mean atomic densities $\bar{n}$ around a few 10^{11} atoms/cm^3, the exchange rate of the SSR mechanism $\omega_{\mathrm{ex}} = \frac{4\pi\hbar}{m} a_{12}\bar{n}$ (where a_{12} is the interstate scattering length and m the mass of ^{87}Rb) becomes larger than the typical dephasing rate and results in a nonlinear collisional shift. We show that the interplay between this nonlinear shift, the differential collisional shift, and the frequency chirp induced by inhomogeneities leads to the existence of a singular operating point for which the clock transition is first-order insensitive to atomic density fluctuations. Operating a quantum sensor in this regime, that we name "magic density," could lead to an increased stability: a key feature in a wide range of precision measurements based on cold atoms such as clocks based on optical pumping

[*]Present address: Kirchhoff-Institut für Physik, Universität Heidelberg, Im Neuenheimer Feld 227, 69120 Heidelberg, Germany.
[†]Present address: Department of Physics and Astronomy, Aarhus University, DK-8000 Aarhus C, Denmark.
[‡]franck.pereira@obspm.fr

and coherent population trapping (CPT) effects [43]. This stability may also find many applications in other fields, such as possible realizations of cold atom quantum memories [44]. A numerical model, developed previously [45], based on coupled Bloch equations of motion for energy-dependent spin vectors qualitatively captures the physics of the problem.

The paper is organized as follows: In Sec. II, the physical system under study and the experimental setup are described. In Sec. III, we study the evolution of the contrast, as well as of the center frequency of the Ramsey fringes versus Ramsey time and atomic density. We observe and discuss the existence of a magic density and introduce the numerical model used to reproduce our experimental data.

II. PHYSICAL SYSTEM AND EXPERIMENTAL SETUP

In our system, described in details in previous work [9,46,47], an ensemble of ^{87}Rb atoms is trapped in a shallow 1D vertical optical lattice with a periodicity of 266 nm. The basis of states can be restricted to two Wannier-Stark ladders associated to the two clock states $|g\rangle = |5s\,^2S_{1/2}, F = 1, m_F = 0\rangle$ and $|e\rangle = |5s\,^2S_{1/2}, F = 2, m_F = 0\rangle$. Indeed, at the shallow depths we operate, only the fundamental Bloch band is populated, the lifetime in higher-order bands being much shorter than the interrogation time. The increment in energy between two consecutive lattice sites is given by the Bloch frequency $\nu_B \approx 568.5$ Hz. A microwave field, resonant with this hyperfine transition $\nu_{HFS} \sim 6.834$ GHz with a Rabi frequency tunable from 1 Hz to a few kHz, allows for a standard clock interrogation: i.e., two $\pi/2$ pulses separated by the Ramsey time T_R.

The experimental setup is described in [48] and is dedicated to the measurement of short-range forces by trapped atom interferometry [20]. Initially, a few 10^8 atoms of ^{87}Rb are trapped within 500 ms in a three-dimensional (3D) magneto-optical trap (MOT) loaded by a two-dimensional (2D)-MOT. After a 100-ms stage of compressed MOT, about 10^7 atoms are transferred into an optical dipole trap realized by two crossed beams at $\lambda = 1070$ nm with waists of 30 and 200 μm and maximum powers of 10 and 20 W, respectively. Evaporative cooling is performed by ramping down the power exponentially to typically 0.1 and 0.25 W within 2 s. The evaporation is stopped just before quantum degeneracy, and a few 10^4–10^5 atoms with a temperature in the range 100–500 nK are then adiabatically loaded within 100 ms in the vertical lattice. During evaporation, a sequence of optical pumping, microwave pulses, and pushing beams polarizes the atomic sample in the state $|F = 1, m_F = 0\rangle$ with more than 99% efficiency. The vertical lattice is realized by retroreflecting a 532-nm laser beam with 500 μm waist and maximal power of 6 W. The transverse confinement is provided by superimposing to the lattice a red detuned progressive wave ($\lambda = 1064$ nm, $0.2 < P_{IR} < 2$ W, waist of 100 μm), giving a maximum radial trapping frequency of $\nu_{rad} \sim 45$ Hz. Finally, a cloud of few 10^4 atoms with a transverse size of 40 μm and a vertical size estimated to a few micrometers is obtained. The mean atomic density $\bar{n}$ can then be varied from 1×10^{11} atoms/cm^3 to few 10^{12} atoms/cm^3 by changing the 2D-MOT loading time.

We explore here the nondegenerate and collisionless Knudsen regime where the trap frequencies are much larger than the lateral collisions rate γ_c. This rate of velocity-changing elastic collisions is given by $\gamma_c \sim 4\pi a^2 v_T \bar{n}$, where a is the scattering length and $v_T = \sqrt{k_B T/m}$ is the atom's thermal velocity, corresponding to typically $0.3\,s^{-1} \ll \nu_{rad}$ in our conditions.

After Ramsey interrogation, the atoms are released from the trap and the populations N_g and N_e in both hyperfine states are counted via state-selective detection based on fluorescence in horizontal light sheets at the bottom of the vacuum chamber. We then compute the transition probability from $|g\rangle$ to $|e\rangle$: $P = \frac{N_e}{N_g+N_e}$, which depends sinusoidally on the phase difference accumulated during the Ramsey sequence. The clock frequency is extracted by scanning the frequency of the interrogation microwave field.

III. EXISTENCE OF A MAGIC DENSITY

For the SSR mechanism to occur, three conditions are required: (i) the system has to be in the Knudsen regime; (ii) the inhomogeneity of the transition, i.e., the inhomogeneous dephasing rate Δ, must be smaller than the exchange rate ω_{ex}; and (iii) the rate of lateral collisions γ_c must be smaller than the exchange rate so that the rephasing arises before atoms are scattered in different energy classes.

Following the qualitative two-macrospins model introduced in [38], the SSR mechanism can be readily depicted. The atoms are here divided into two energy classes. After the first $\pi/2$ pulse, these two classes have different transverse spin precession rates because they experience different potentials. In the absence of lateral collision, atoms do not change class and dephase. In the presence of collective and cumulative ISRE, the two classes rephase after an exchange period $T_{ex} = 2\pi/\omega_{ex}$ (see [41], Fig. 2, for a representation on the Bloch sphere). This dynamics can also be interpreted by analyzing the system in the singlet-triplet basis of the two-spin states [39].

A. Theoretical model and approximations

For a more quantitative study of the spin dynamics, we use the model of [38,41,45]. There, the motion of atoms in the trap is treated semiclassically. In the Knudsen regime ($\gamma_c \ll \nu_{rad}$), the atoms undergo many oscillations in the trap between two lateral collisions, which allows us to group the atoms according to their motional energy E. The spin dynamics is then described with coupled Bloch equations of motion for energy-dependent spin vectors $\mathbf{S}(E,t)$, with E in units of $k_B T$:

$$\partial_t \mathbf{S}(E,t) \approx [\Delta(E)\hat{\mathbf{w}} + \omega_{ex}\bar{\mathbf{S}}(t)]\mathbf{S}(E,t) - \gamma_c[\mathbf{S}(E,t) - \bar{\mathbf{S}}(t)], \quad (1)$$

where $\bar{\mathbf{S}}(t) = \int_0^\infty dE' g(E')\mathbf{S}(E',t)$ is the energy-average spin [$g(E)$ is the density of states], and $\hat{\mathbf{w}}$ is the vertical unit vector of the Bloch sphere. In our experiment, the dephasing $\Delta(E)$ is dominated by the second-order Zeeman shift due to the vertical bias field, the differential ac-Stark shift of the transverse trapping laser, and the mean-field (MF) shift. It is given by

$$\Delta(E) = \delta^{Z2} + (\delta^{ac} + \Delta^{ac}E) + \Delta^{MF}e^{-E/2}. \quad (2)$$

The magnetic field, whose inhomogeneity is negligible across the cloud, gives rise to a homogeneous dephasing of $\delta^{Z2}/2\pi = 5.7$ Hz for our vertical bias field of 100 mG. The transverse optical potential can be approximated by a 2D harmonic oscillator. The dephasing due to ac-Stark shift is then linear with E, the homogeneous part is given by $\delta^{ac}/2\pi = -2.15$ Hz [49], and the inhomogeneous part by $\Delta^{ac}/2\pi = 0.17$ Hz [50]. Regarding the dynamics in the vertical direction, it is considered to be frozen, as the atomic wave packets remain in the fundamental band of the optical lattice [they actually undergo Bloch oscillations at a large pulsation compared to $\Delta(E)$]. By considering a 3D Gaussian profile for the atomic density, the dephasing due to the mean-field shift exhibits an exponential dependence with E. Its amplitude is approximated by $\Delta^{MF} \sim \frac{9\sqrt{2}}{4}\frac{4\pi\hbar}{m}(a_{22} - a_{11})\bar{n} \sim -2\pi \times 0.16\bar{n}$ Hz (cf. Appendix), where $\bar{n}$ is expressed in units of 10^{11} atoms/cm^3, and a_{ii} are the scattering lengths for atoms in the state $|F = i, m_F = 0\rangle$.

The second term in Eq. (1), nonlinear spin density, represents the exchange mean field due to ISRE and is responsible for the SSR mechanism. The last term in Eq. (1) is the effective spin relaxation due to lateral collisions.

An ensemble of independent wells is considered and the dynamics in each well is modeled using Eq. (1). Indeed, no collision event is likely to change the vertical motional state of an atom, as the energy scale of atom-atom interactions is low compared to the Bloch frequency. The population of the different wells is assumed to follow an initial Gaussian density distribution in z.

At a given evolution time T_R and after a homogeneous $\pi/2$ pulse, as the energy-average spin $\bar{\mathbf{S}}(T_R)$ stands in the equatorial plane of the Bloch sphere, we can then directly derive the contrast $C(T_R) = |\bar{\mathbf{S}}(T_R)|$ and the frequency measured by Ramsey spectroscopy $\nu(T_R) = \arg[\bar{\mathbf{S}}(T_R)]/2\pi T_R$.

B. Study of the coherence

In a first series of experiments, we study the contrast of Ramsey interferometers as it is needed to investigate how the SSR mechanism is at play in the 1D vertical lattice and to extract the relevant parameters required for the following simulations. The contrast is extracted from the envelope of the Ramsey fringes, which are obtained by scanning both the Ramsey time and the phase of the exciting field. The evolution of the contrast in the lattice for different atomic densities is shown in Fig. 1. It follows the same trend already observed in single-well magnetic and optical dipole traps [38,40,41]: the contrast initially drops because of inhomogeneities and then stabilizes at a value which increases with $\bar{n}$ thanks to SSR. Nevertheless, no clear contrast revivals at the exchange period are observed here, which can be explained by the fact that all the wells are independent from each other. This leads to a Gaussian distribution of $\omega_{ex}(z)$, which damps the contrast revivals by averaging over the cloud.

As shown in Fig. 1, our numerical model (solid lines) reproduces well the behavior of the experimental curves. Nevertheless, as there is no sharp contrast revival and the adjustment of the fit parameters is more delicate than in previous experiments [38,40,41], as they are not completely independent. The final set of fitting parameters gives us

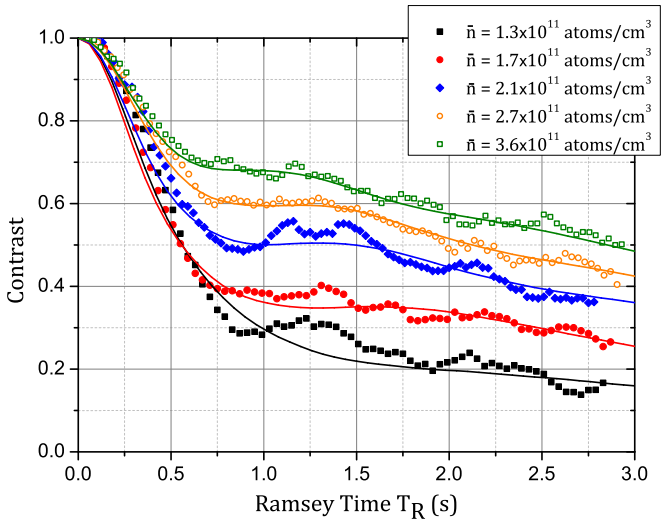

FIG. 1. Contrast vs Ramsey time T_R for different mean atomic densities $\bar{n}$. For large T_R, the contrast increases when $\bar{n}$ increases as a consequence of spin self-rephasing. The solid lines correspond to fit according to Eq. (1), with ω_{ex}, γ_c, Δ^{ac}, and Δ^{MF} as free fitting parameters.

$\omega_{ex}/2\pi = 0.32(2) \times \bar{n}$ Hz and $\gamma_c = 0.040(4) \times \bar{n}\,\mathrm{s}^{-1}$. These values are respectively smaller by a factor 0.6 and 0.3 than the expected values. This fact, also observed in [38,40,41], is a consequence of the infinite range approximation taken for these two contributions in Eq. (1) which overestimates their effects. We obtain for the inhomogeneity parameters $\Delta^{ac}/2\pi = 0.24(5)$ Hz, larger than expected, and $\Delta^{MF}/2\pi = 0.40(8)$ Hz, with no clear dependence on density.

As with previous experiments based on single-well traps [38,40,41], this model allows for a good understanding of the coherence of our self-rephasing ensemble of ultracold atoms trapped in a 1D lattice. In the following, we further compare this model to our experimental measurement of the center frequency and show that it also reproduces the existence of a magic density.

C. Study of the frequency

In our system, three main contributions affect the evolution of the frequency of the hyperfine transition during a Ramsey sequence:

(i) Atomic interactions lead to an offset of the clock frequency. It can be evaluated by computing the average mean-field shift $\bar{\Delta}^{MF}/2\pi = -0.05\bar{n}$. This collisional shift is negative, as $a_{22} < a_{11}$ for ^{87}Rb.

(ii) The inhomogeneous dephasing gives rise to a chirp of the clock frequency [51]. The direction of this chirp depends on the sign of the inhomogeneous dephasing. In our density regime, the observed down-chirp is mainly due to $\Delta^{ac} > 0$ [52].

(iii) The collective SSR mechanism counteracts dephasing [38,40,41] and keeps atoms synchronized. Then for Ramsey times $T_R > T_{ex}$, the chirp induced by the inhomogeneous dephasing is inhibited and the clock frequency remains constant.

From Eq. (1), the numerical derivation of the clock frequency as a function of the Ramsey time is depicted in

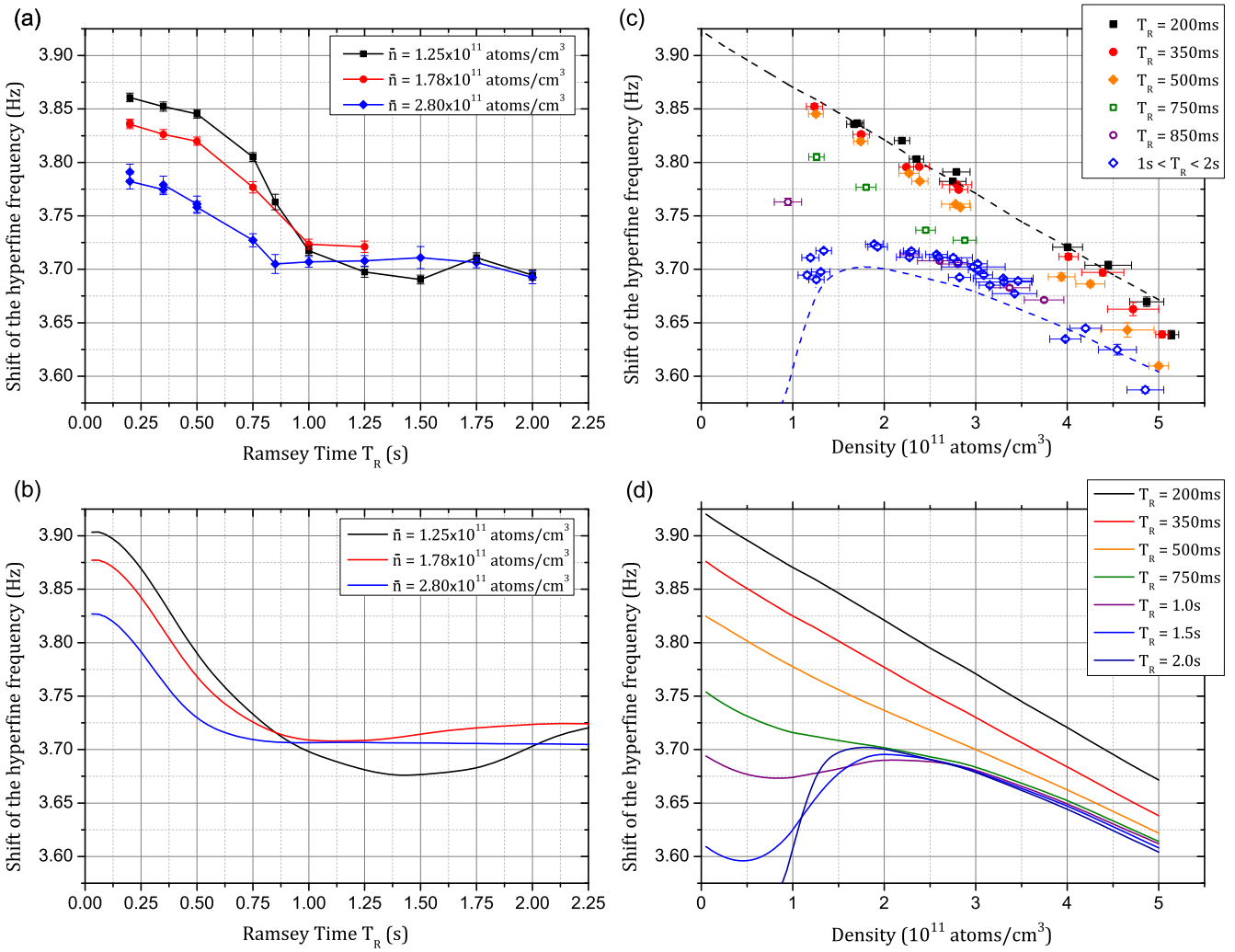

FIG. 2. Magic density. (a) Frequency shift as a function of the Ramsey time for three different values of the atomic density and (b) curves obtained from the numerical model. (c) Frequency shift as a function of the atomic density for different values of the Ramsey time and (d) curves obtained from the numerical model; in (c) the two dashed lines correspond to numerical model for $T_R = 200$ ms and $T_R = 2$ s. The values of the model's parameters ω_{ex}, γ_c, Δ^{ac}, and Δ^{MF} are discussed in the text. The value of the frequency shift at the origin in (a) and (b) is given by the sum of the homogeneous dephasing and the average of the inhomogeneous part: $\delta^{Z2} + \delta^{ac} + 2\Delta^{ac} + \bar{\Delta}^{MF}$.

Fig. 2(b) for three values of the mean atomic density $\bar{n} = \{1.25, 1.78, 2.80\} \times 10^{11}$ atoms/cm^3. The three previous contributions to the clock frequency can be clearly observed. First, the collisional shift creates a negative offset at $T_R = 0$ which increases linearly with the density. Second, the inhomogeneity $\Delta(E)$ begets a down-chirp which is, thirdly, counterbalanced by the effect of exchange interactions. The larger the density, the shorter the Ramsey time at which this happens. These simulations are in good agreement with the experimental results shown in Fig. 2(a) (the values of the parameters ω_{ex}, γ_c, Δ^{ac}, and Δ^{MF} are discussed later). We can notice the existence of crossing points between the curves for different $\bar{n}$ at given values of T_R. At these singular operating points, the clock frequency is identical for two different densities and there thus exists in their vicinity a "magic density" where the clock frequency is insensitive at first order to density fluctuations. We can also notice that for the highest density $\bar{n} = 2.8 \times 10^{11}$ atoms/cm^3, where the SSR mechanism is the most efficient, when $T_R > T_{ex}$, the clock frequency remains very stable with the Ramsey time.

In the following paragraph, we qualitatively discuss a necessary condition for the existence of a magic density. Here, we consider the evolution of the clock frequency as a function of the Ramsey time for two atomic ensembles with different densities $\bar{n}_1 < \bar{n}_2$ and whose inhomogeneities $\Delta(E)$ are equivalent [see Fig. 2(b)]. Because of SSR, the chirp induced by the inhomogeneous dephasing is stopped at shorter Ramsey time for the highest density $\bar{n}_2$. In these conditions, if we consider a down-chirp, a negative collisional shift $\bar{\Delta}^{MF}$ is necessary to obtain a crossing point (and inversely for an up-chirp). In our conditions, the sign of the collisional shift and of Δ^{ac}, which is the main source of the chirp, must thus be opposite for the existence of a magic density.

In a second series of experiments, we measure the clock frequency as a function of the atomic density for different Ramsey times [cf. Fig. 2(c)]. The atomic density is evaluated by measuring the collisional shift $\bar{\Delta}^{MF}$ with Ramsey spectroscopy at short $T_R < T_{ex}$. As suggested by the previous results [cf. Figs. 2(a) and 2(b)], for $T_R < 0.8$ s, there is no crossing point between curves for different $\bar{n}$ and so the collisional

shift remains monotonic and no magic density is observed. For $T_R > 0.8$ s, there exist different crossing points, and when $T_R > 1$ s, all the curves for $1 < \bar{n} < 3 \times 10^{11}$ atoms/cm^3 essentially converge on the same constant frequency shift. In these conditions, a nonmonotonic collisional shift is expected and indeed, a magic density is clearly observed at around $\bar{n} \sim 1.8 \times 10^{11}$ atoms/cm^3 for $T_R > 1$ s. In Figs. 2(c) and 2(d), the measurements are qualitatively in good agreement with the numerical model.

Solid lines in Figs. 2(c) and 2(d) are numerical evaluations of Eq. (1) using only one free fitting parameter Δ^{ac}. ω_{ex} and γ_c are extracted from the fit of the contrast study presented in Fig. 1. Δ^{MF} is set to its expected value $-2\pi \times 0.16\bar{n}$ Hz. We obtain $\Delta^{\mathrm{ac}}/2\pi = 0.30(2)$ Hz, larger than the expected value, as in the contrast study.

IV. CONCLUSION

We have shown that the interplay between inhomogeneous dephasing, collisional shift, and exchange interaction leads to the existence of a magic density if the sign of inhomogeneous dephasing due to the ac-Stark shift is opposite to that of the collisional shift. This singular phenomenon, which occurs at an intermediate density regime for which spin self-rephasing starts to counteract the frequency chirp induced by inhomogeneous dephasing, is well reproduced by a numerical model based on coupled Bloch equations of motion for energy-dependent spin vectors. The existence of these singular operating points, where the clock transition is insensitive to density fluctuations, is a promising tool to increase the stability and the sensitivity of atomic sensors by tackling one of today's main limitations in atomic clocks based on trapped ultracold atoms. The current relative accuracy on the clock frequency measured in our system (initially not dedicated to perform high-precision spectroscopy of internal degrees of freedom) is at a level of a few 10^{-12}. An improved numerical model and a careful survey of the SSR mechanism in state-of-the-art atomic clocks are consequently necessary for a competitive accurate time-keeping using the magic density. Nevertheless, the potentially improved stability is of great interest in a wide range of precision measurements, e.g., CPT clocks, and other applications, e.g., atom quantum memories, based on cold atoms.

Finally, the magic density can be adjusted, in principle, by tuning the inhomogeneities in order to find a working point at both a large Ramsey time and a large number of atoms. This would allow one to reduce the deleterious impact of density fluctuations while preserving a high sensitivity and a low standard quantum limit. In magnetic traps, for instance, the inhomogeneity can be easily tuned by varying the magnetic field at the bottom of the trap away from its magic value. This was done at SYRTE in the trapped atomic clock on a chip experiment [25] to study the dependence of the magic density on the inhomogeneity [53]. In our experiment, the differential light shift inhomogeneity cannot be easily varied (for instance, by changing the laser power) without modifying the size of the cloud and thus the density. Instead, we could use Raman laser beams in a counterpropagating configuration. For a sufficiently low lattice depth, two-photon Raman transitions can coherently and selectively couple given lattice sites thanks to laser-induced tunneling [46]. In these conditions, a $\pi/2$ Raman pulse can be used to shift the atoms in $|F = 2\rangle$ by a given number of lattice sites with respect to the atoms in $|F = 1\rangle$. This would allow for fine control of the spatial overlap between trapped atomic wave packets in each internal state, for a subsequent fine tuning of the value of $\omega_{\mathrm{ex}} \propto a_{12}\bar{n}$ and thus potentially of the magic density.

ACKNOWLEDGMENTS

We thank F. Combes, J.-N. Fuchs, and F. Piéchon for insightful discussions and for providing us the code of the numerical model. We also thank P. Rosenbush, W. Maineult, and K. Gibble for useful discussions. We acknowledge financial support by the IDEX PSL (ANR-10-IDEX-001-02 PSL) and ANR (ANR-13-BS04-0003-01). A. Bonnin thanks the Labex First-TF for financial support.

APPENDIX: DEPHASING DUE TO MEAN-FIELD SHIFT

It is more convenient to study the spin dynamics in phase space using the energy-angle variables E, α instead of the usual position-momentum variables [38]. In this space under the approximations of a frozen dynamics in z and a 3D Gaussian profile of the atomic density, the dephasing due to the mean-field shift is expressed as

$$\begin{aligned}
&\Delta^{\mathrm{MF}}(z, E) \\
&= \frac{4\pi\hbar}{m}(a_{22} - a_{11}) n_0 e^{-z^2/2\sigma_z^2} \left(\prod_{i=x,y} \int_0^{2\pi} \frac{d\alpha_i}{2\pi} e^{-E_i \cos^2(\alpha_i)} \right) \\
&= \frac{4\pi\hbar}{m}(a_{22} - a_{11}) n_0 e^{-z^2/2\sigma_z^2} e^{-E/2} \left(\prod_{i=x,y} I_0\left(\frac{E_i}{2}\right) \right) \\
&\simeq \frac{4\pi\hbar}{m}(a_{22} - a_{11}) n_0 e^{-z^2/2\sigma_z^2} e^{-E/2}, \qquad \text{(A1)}
\end{aligned}$$

where n_0 is the peak atomic density, σ_z the width of the atomic density distribution in the vertical direction, and I_0 the Bessel function of the first kind, which we have neglected. We have verified that this approximation leads to negligible corrections when we adjust the model parameters so as to match with experimental results. Finally, it is convenient to express this dephasing as a function of $\bar{n}$, which is directly accessible by measuring the collisional shift. By averaging the density profile over the vertical atomic distribution and the 2D energy distribution we obtain $n_0 = \frac{9\sqrt{2}}{4}\bar{n}$.

[1] P. O. Schmidt, T. Rosenband, C. Langer, W. M. Itano, J. C. Bergquist, and D. J. Wineland, Spectroscopy using quantum logic, Science **309**, 749 (2005).

[2] J. H. Lee, E. Montano, I. H Deutsch, and P. S. Jessen, Robust site-resolvable quantum gates in an optical lattice via inhomogeneous control, Nat. Commun. **4**, 2027 (2013).

[3] I. Bloch, J. Dalibard, and S. Nascimbène, Quantumsimulations with ultracold quantum gases, Nat. Phys. **8**, 267 (2012).

[4] I. Ushijima, M. Takamoto, M. Das, T. Ohkubo, and H. Katori, Cryogenic optical lattice clocks, Nat. Photonics **9**, 185 (2015).

[5] T. L. Nicholson, S. L. Campbell, R. B. Hutson, G. E. Marti, B. J. Bloom, R. L. McNally, W. Zhang, M. D. Barrett, M. S. Safronova, G. F. Strouse, W. L. Tew, and J. Ye, Systematic evaluation of an atomic clock at 2×10^{-18} total uncertainty, Nat. Commun. **6**, 6896 (2015).

[6] M. Schioppo, R. C. Brown, W. F. McGrew, N. Hinkley, R. J. Fasano, K. Beloy, T. H. Yoon, G. Milani, D. Nicolodi, J. A. Sherman, N. B. Phillips, C. W. Oates, and A. D. Ludlow, Ultrastable optical clock with two cold-atom ensembles, Nat. Photonics **11**, 48 (2016).

[7] S. L. Campbell, R. B. Hutson, G. E. Marti, A. Goban, N. Darkwah Oppong, R. L. McNally, L. Sonderhouse, J. M. Robinson, W. Zhang, B. J. Bloom, and J. Ye, A Fermi-degenerate three-dimensional optical lattice clock, Science **358**, 90 (2017).

[8] N. Poli, F.-Y. Wang, M. G. Tarallo, A. Alberti, M. Prevedelli, and G. M. Tino, Precision Measurement of Gravity with Cold Atoms in an Optical Lattice and Comparison with a Classical Gravimeter, Phys. Rev. Lett. **106**, 038501 (2011).

[9] A. Hilico, C. Solaro, M.-K. Zhou, M. Lopez, and F. Pereira dos Santos, Contrast decay in a trapped-atom interferometer, Phys. Rev. A **91**, 053616 (2015).

[10] G. Ranjit, M. Cunningham, K. Casey, and A. A. Geraci, Zeptonewton force sensing with nanosphere in optical lattice, Phys. Rev. A **93**, 053801 (2016).

[11] A. M. Rey, A. V. Gorshkov, and C. Rubbo, Many-Body Treatment of the Collisional Frequency Shift in Fermionic Atoms, Phys. Rev. Lett. **103**, 260402 (2009).

[12] M. Bishof, Y. Lin, M. D. Swallows, A. V. Gorshkov, J. Ye, and A. M. Rey, Resolved Atomic Interaction Sidebands in an Optical Clock Transition, Phys. Rev. Lett. **106**, 250801 (2011).

[13] M. J. Martin, M. Bishof, M. D. Swallows, X. Zhang, C. Benko, J. von Stecher, A. V. Gorshkov, A. M. Rey, and Jun Ye, A quantum many-body spin system in an optical lattice clock, Science **341**, 632 (2013).

[14] M. G. Tarallo, T. Mazzoni, N. Poli, D. V. Sutyrin, X. Zhang, and G. M. Tino, Test of Einstein Equivalence Principle for 0-Spin and Half-Integer-Spin Atoms: Search for Spin-Gravity Coupling Effects, Phys. Rev. Lett. **113**, 023005 (2014).

[15] P. Delva, J. Lodewyck, S. Bilicki, E. Bookjans, G. Vallet, R. Le Targat, P.-E. Pottie, C. Guerlin, F. Meynadier, C. Le Poncin-Lafitte, O. Lopez, A. Amy-Klein, W.-K. Lee, N. Quintin, C. Lisdat, A. Al-Masoudi, S. Dörscher, C. Grebing, G. Grosche, A. Kuhl, S. Raupach, U. Sterr, I. R. Hill, R. Hobson, W. Bowden, J. Kronjäger, G. Marra, A. Rolland, F. N. Baynes, H. S. Margolis, and P. Gill, Test of Special Relativity Using a Fiber Network of Optical Clocks, Phys. Rev. Lett. **118**, 221102 (2017).

[16] R. M. Godun, P. B. R. Nisbet-Jones, J. M. Jones, S. A. King, L. A. M. Johnson, H. S. Margolis, K. Szymaniec, S. N. Lea, K. Bongs, and P. Gill, Frequency Ratio of Two Optical Clock Transitions in Yb+171 and Constraints on the Time Variation of Fundamental Constants, Phys. Rev. Lett. **113**, 210801 (2014).

[17] A. Hees, J. Guéna, M. Abgrall, S. Bize, and P. Wolf, Searching for an Oscillating Massive Scalar Field as a Dark Matter Candidate Using Atomic Hyperfine Frequency Comparisons, Phys. Rev. Lett. **117**, 061301 (2016).

[18] S. Dimopoulos and A. A. Geraci, Probing submicron forces by interferometry of Bose-Einstein condensed atoms, Phys. Rev. D **68**, 124021 (2003).

[19] I. Carusotto, L. Pitaevskii, S. Stringari, G. Modugno, and M. Inguscio, Sensitive Measurement of Forces at the Micron Scale using Bloch Oscillations of Ultracold Atoms, Phys. Rev. Lett. **95**, 093202 (2005).

[20] R. Messina, S. Pelisson, M.-C. Angonin, and P. Wolf, Atomic states in optical traps near a planar surface, Phys. Rev. A **83**, 052111 (2011).

[21] M. Takamoto, F.-L. Hong, R. Higashi, and Hidetoshi Katori, An optical lattice clock, Nature (London) **435**, 321 (2005).

[22] Jun Ye, H. J. Kimble, and Hidetoshi Katori, Quantum state engineering and precision metrology using state-insensitive light traps, Science **320**, 1734 (2008).

[23] A. Derevianko, "Doubly Magic" Conditions in Magic-Wavelength Trapping of Ultracold Alkali-Metal Atoms, Phys. Rev. Lett. **105**, 033002 (2010).

[24] L. Sárkány, P. Weiss, H. Hatterman, and J. Fortágh, Controlling the magnetic-field sensitivity of atomic-clock states by microwave dressing, Phys. Rev. A **90**, 053416 (2014).

[25] R. Szmuk, V. Dugrain, W. Maineult, J. Reichel, and P. Rosenbusch, Stability of a trapped-atom clock on a chip, Phys. Rev. A **92**, 012106 (2015).

[26] W. M. Itano, J. C. Bergquist, J. J. Bollinger, J. M. Gilligan, D. J. Heinzen, F. L. Moore, M. G. Raizen, and D. J. Wineland, Quantum projection noise: Population fluctuations in two-level systems, Phys. Rev. A **47**, 3554 (1993).

[27] D. M. Harber, H. J. Lewandowski, J. M. McGuirk, and E. A. Cornell, Effect of cold collisions on spin coherence and resonance shifts in a magnetically trapped ultracold gas, Phys. Rev. A **66**, 053616 (2002).

[28] R. Jannin, P. Cladé, and S. Guellati-Khélifa, Phase shift due to atom-atom interactions in a light-pulse atom interferometer, Phys. Rev. A **92**, 013616 (2015).

[29] G. K. Campbell, M. M. Boyd, J. W. Thomsen, M. J. Martin, S. Blatt, M. D. Swallows, T. L. Nicholson, T. Fortier, C. W. Oates, S. A. Diddams, N. D. Lemke, P. Naidon, P. Julienne, Jun Ye, and A. D. Ludlow, Probing interactions between ultracold fermions, Science **324**, 360 (2009).

[30] K. Gibble, Decoherence and Collisional Frequency Shifts of Trapped Bosons and Fermions, Phys. Rev. Lett. **103**, 113202 (2009).

[31] Z. Yu and C. J. Pethick, Clock Shifts of Optical Transitions in Ultracold Atomic Gases, Phys. Rev. Lett. **104**, 010801 (2010).

[32] W. Maineult, C. Deutsch, K. Gibble, J. Reichel, and P. Rosenbusch, Spin Waves and Collisional Frequency Shifts of a Trapped-Atom Clock, Phys. Rev. Lett. **109**, 020407 (2012).

[33] Eric L. Hazlett, Yi Zhang, Ronald W. Stites, Kurt Gibble, and Kenneth M. O'Hara, S-Wave Collisional Frequency Shift of a Fermion Clock, Phys. Rev. Lett. **110**, 160801 (2013).

[34] S. Lee, C. Yong Park, W.-K. Lee, and D.-H. Yu, Cancellation of collisional frequency shifts in optical lattice clocks with Rabi spectroscopy, New J. Phys. **18**, 033030 (2016).

[35] M. D. Swallows, M. Bishof, Y. Lin, S. Blatt, M. J. Martin, A. M. Rey, and J. Ye, Suppression of collisional shifts in a strongly interacting lattice clock, Science **331**, 1043 (2011).

[36] C. Gross, T. Zibold, E. Nicklas, J. Estève, and M. K. Oberthaler, Nonlinear atom interferometer surpasses classical precision limit, Nature (London) **464**, 1165 (2010).

[37] Y. Sagi, I. Almog, and N. Davidson, Universal Scaling of Collisional Spectral Narrowing in an Ensemble of Cold Atoms, Phys. Rev. Lett. **105**, 093001 (2010).

[38] C. Deutsch, F. Ramirez-Martinez, C. Lacroûte, F. Reinhard, T. Schneider, J. N. Fuchs, F. Piéchon, F. Laloë, J. Reichel, and P. Rosenbusch, Spin Self-Rephasing and Very Long Coherence Times in a Trapped Atomic Ensemble, Phys. Rev. Lett. **105**, 020401 (2010).

[39] K. Gibble, Keeping atoms synchronized for better timekeeping, Physics **3**, 55 (2010).

[40] G. Kleine Büning, J. Will, W. Ertmer, E. Rasel, J. Arlt, C. Klempt, F. Ramirez-Martinez, F. Piéchon, and P. Rosenbusch, Extended Coherence Time on the Clock Transition of Optically Trapped Rubidium, Phys. Rev. Lett. **106**, 240801 (2011).

[41] C. Solaro, A. Bonnin, F. Combes, M. Lopez, X. Alauze, J.-N. Fuchs, F. Piéchon, and F. Pereira dos Santos, Competition Between Spin Echo and Spin Self-Rephasing in a Trapped Atom Interferometer, Phys. Rev. Lett. **117**, 163003 (2016).

[42] C. Lhuillier and F. Laloë, Transport properties in a spin polarized gas, I, J. Phys. (France) **43**, 197 (1982).

[43] S. Knappe, V. Gerginov, P. D. D. Schwindt, V. Shah, H. G. Robinson, L. Hollberg, and J. Kitching, Atomic vapo cells for chip-scale atomic clocks with improved long-term frequency stability, Opt. Lett. **30**, 2351 (2005).

[44] S. Bernon, H. Hattermann, D. Bothner, M. Knufinke, P. Weiss, F. Jessen, D. Cano, M. Kemmler, R. Kleiner, D. Koelle, and J. Fortágh, Manipulation and coherence of ultra-cold atoms on a superconducting atom chip, Nat. Commun. **4**, 2380 (2013).

[45] F. Piéchon, J.-N. Fuchs, and F. Laloë, Cumulative Identical Spin Rotation Effects in Collisionless Trapped Atomic Gases, Phys. Rev. Lett. **102**, 215301 (2009).

[46] Q. Beaufils, G. Tackmann, X. Wang, B. Pelle, S. Pelisson, P. Wold, and F. Pereira dos Santos, Laser Controlled Tunneling in a Vertical Optical Lattice, Phys. Rev. Lett. **106**, 213002 (2001).

[47] B. Pelle, A. Hilico, G. Tackmann, Q. Beaufils, and F. Pereira dos Santos, State-labeling Wannier-Stark atomic interferometers, Phys. Rev. A **87**, 023601 (2013).

[48] X. Alauze, A. Bonnin, C. Solaro, and F. Pereira dos Santos, A trapped ultracold atom force sensor with a μm-scale spatial resolution, New J. Phys. **20**, 083014 (2018).

[49] δ^{ac} is given by $(U_0^{F=2} - U_0^{F=1})/\hbar$, where $U_0^{F=i}$ is the trapping potential of the transverse laser experienced by an atom in $F = i$, $i \in \{1, 2\}$.

[50] In the harmonic approximation, Δ^{ac} is given by $\frac{k_B T}{2\hbar} \times \frac{\delta\alpha}{\alpha}$ [41,51], where $\delta\alpha$ and α are the differential and the total light shift per intensity.

[51] S. Kuhr, W. Alt, D. Schrader, I. Dotsenko, Y. Miroshnychenko, A. Rauschenbeutel, and D. Meschede, Analysis of dephasing mechanisms in a standing-wave dipole trap, Phys. Rev. A **72**, 023406 (2005).

[52] In the Knudsen regime and without exchange interaction, the energy-average spin vector evolves in the equatorial plane of the Bloch sphere and can be expressed as $\overline{\mathbf{S}}(T_R) = S_x + iS_y = \int_0^\infty g(E)\exp(i\Delta^{\mathrm{ac}} E T_R) dE = (1 - i\Delta^{\mathrm{ac}} T_R)^{-d}$, where d is the dimension of the problem. In 2D this evolution leads to a down-chirp given by $\frac{2}{2\pi T_R}\arctan(\Delta^{\mathrm{ac}} T_R)$.

[53] C. Deutsch, Trapped atom clock on a chip–Identical spin rotation effects in an ultracold trapped atomic clock, Ph.D. thesis, Université Pierre et Marie Curie, 2011.